Local Structure Invariant Potential for $In_xGa_{1-x}As$ Semiconductor Alloys

Eunji Sim,[†,*] Minwoo Han,[†] Joost Beckers,[‡] and Simon de Leeuw[§]

[†]*Department of Chemistry and Institute of NanoBio Molecular Assemblies, Yonsei University, Seoul 120-749, Korea*
[*]*E-mail: esim@yonsei.ac.kr.*
[‡]*Computational Physics, Faculty of Applied Sciences, Delft University of Technology, Julianalaan 136, 2628 BL Delft, the Netherlands*
[§]*Gorlaeus Laboratories, Leiden Institute of Chemistry, Einsteinweg 55, 2333 CC Leiden, the Netherlands*
Received January 22, 2009, Accepted February 21, 2009

We model lattice-mismatched group III-V semiconductor $In_xGa_{1-x}As$ alloys with the three-parameter anharmonic Kirkwood-Keating potential, which includes realistic distortion effect by introducing anharmonicity. Although the potential parameters were determined based on optical properties of the binary parent alloys InAs and GaAs, simulated dielectric functions, reflectance, and Raman spectra of alloys agree excellently with experimental data for any arbitrary atomic composition. For a wide range of atomic composition, InAs- and GaAs-bond retain their respective properties of binary parent crystals despite lattice and charge mismatch. It implies that use of the anharmonic Kirkwood-Keating potential may provide an optimal model system to investigate diverse and unique optical properties of quantum dot heterostructures by circumventing potential parameter searches for particular local structures.

Key Words: Alloys, Semiconductors, Empirical potential, Molecular dynamics simulation, Quantum well structures

Introduction

Recently tremendous interest has been drawn to optical behaviours of semiconductor quantum dots (QDs). Unique optical properties of QDs that strongly depend on the size and shape are considered to be important in the wide range of potential applications, such as biomedical imaging,[1,2] infrared optical devices,[3,4] and quantum information processors.[5] Particularly interesting is an infrared light-emitting QDs in the wavelength range of 800 and 900 nm, where absorption in tissue is minimal. While cadmium-based QDs have been most intensively investigated, recent developments have shown that indium-based semiconductor QDs are considered a better choice that can work for *in vivo* imaging applications, as demonstrated by Bawendi group.[1,2] By using varying proportions of the materials and changing synthesis procedures, each layer of a quantum well may have a different composition fraction of $A_xB_{1-x}C$ type semiconductors or even different atoms to neighbouring layers and, in turn, emission structure can be altered.[6,7]

Successful implementation of QD applications requires easy manipulation of the selectivity and tuneability of optical and electrical properties of nanoscale QD systems. In order to design and synthesize QDs with desired properties, theoretical tools that can model QD systems are extremely beneficial. Although QD structures are relevantly new to the community, alloy forms of group III-V semiconductors, such as $In_xGa_{1-x}As$, have been investigated extensively both experimentally[8,9,10,11,12] and theoretically.[13,14,15] Theoretical understanding of QD properties is established with the development of the potential, which can accurately describe particle-particle interactions within structure, which in turn give rise to their unique properties. Since the properties of QDs are highly sensitive to the size and shape of their structures, it is advantageous to have a model system whose potential parameters are rather insensitive to the local structures. In addition, the model system is desired to be easy to generalize and to apply to complex local structures including core/shell heterostructures. In that sense, it is preferable to avoid computationally demanding quantum mechanical calculations and to use empirical potentials whose parameters are determined by molecular mechanical simulations. Therefore, recently developed anharmonic Kirkwood-Keating potential that uses molecular dynamics(MD) simulations may provide an optimal model for QD structures. While potential parameters of alloys are determined based on the dispersion relation and reflectance of the binary parent alloys, the model is easy to implement to any atomic composition of semiconductor alloys.[16]

In this article, we fit the potential parameters of anharmonic Kirkwood-Keating potential for $In_xGa_{1-x}As$ for various atomic compositions and verify that MD simulations based on the fitted model reproduces experimentally observed optical properties of alloys. The article is organized as the followings: In section 2, the anharmonic Kirkwood-Keating model is briefly discussed as well as the compositional dependence of potential parameters. In section 3, the whole composition range is explored using the optimal potential parameters. The direction of future work is discussed in the final section.

Model

The anharmonic Kirkwood-Keating potential model replaces the harmonic bond-stretching term of the Kirkwood-Keating

potential with a Morse potential in order to introduce physical damping effect at finite temperature:[16]

$$V_{strain} = \sum_{<i,j\neq i>} \frac{\alpha_{ij}}{2\left(\chi_{ij}/r_{ij}^0\right)^2}\{e^{-2\frac{\chi_{ij}}{r_{ij}^0}(r_{ij}-r_{ij}^0)} - 2e^{-\frac{\chi_{ij}}{r_{ij}^0}(r_{ij}-r_{ij}^0)} + 1\} + \sum_{<i,j\neq i,k\neq i,j>} \frac{\beta_{ijk} r_{ij}^0 r_{ik}^0}{8}\left(\frac{\vec{r}_{ij}\cdot\vec{r}_{ik}}{r_{ij}r_{ik}} + \frac{1}{3}\right)^2 . \quad (1)$$

Index i runs over all atoms and j and k run over the four nearest neighbours of atom i in tetrahedral structure. r_{ij} is the distance between atoms i and j, while r_{ij}^0 is the equilibrium distance. The Morse bond-stretch term in Eq.(1) is formulated such that, the parameter α_{ij} corresponds to the Kirkwood-Keating harmonic spring constant[17,18] and χ_{ij} determines the degree of anharmonicity. While χ_{ij} is dimensionless, both parameters α_{ij} and β_{ijk} have the dimension of a force constant (N·m^{-1}). The first term in Eq. (1) represents the two-body central force interaction of the covalent bond between Ga-As or In-As, while the second term describes the angular interaction between atom i and its two nearest neighbors j and k.

The Coulomb potential energy is given by

$$V_{coulmb} = \frac{1}{4\pi\varepsilon_0}\sum_{\langle i,j\neq i\rangle}\frac{q_{eff}^i q_{eff}^j}{r_{ij}} , \quad (2)$$

where ε_0 is the vacuum permittivity. q_{eff}^i is the effective charge of atom i, which is defined as $q_{eff}^i = q_i/\sqrt{\varepsilon_\infty}$ with ε_∞ being the high frequency dielectric constant. In general, the long-range forces are important for an exact description of the phonon dispersion. For instance, they cause the longitudinal optical (LO) and transversal optical (TO) phonon frequency to split at the Brillouin zone-centre. In a polar material, in a cubic crystal, only LO displacement produces a macroscopic ionic polarization and the corresponding macroscopic electric field gives rise to an additional restoring force and the LO-TO splitting.[19] The periodic boundary condition was applied to an uneven-surface rectangular sample to avoid a macroscopic electrostatic field. Considering the lattice constants in GaAs and InAs binary crystal are 5.70 Å and 6.05 Å, respectively, the short-range interaction cutoff was chosen to be 8.5 Å between 480 atoms. On the other hand, the long-range Coulomb interaction was taken into account by means of the Ewald sum.[20,21]

Since the parameters of pure GaAs crystals have been thoroughly examined and determined elsewhere,[16] we consider pure InAs crystals. The parameters $\alpha_{\text{In-As}}$ and $\beta_{\text{In-As-In}}$ are fitted to reproduce experimentally measured elastic constants and phonon frequencies using a simple expression for the optical phonon frequency in the limit of long wavelength:[22]

$$\omega_0^h = \sqrt{\frac{4}{3\mu}(\alpha_{In-As} + \frac{16}{9}\beta_{In-As-In})} , \quad (3)$$

where μ is the reduced mass of InAs and ω_0^h is the low

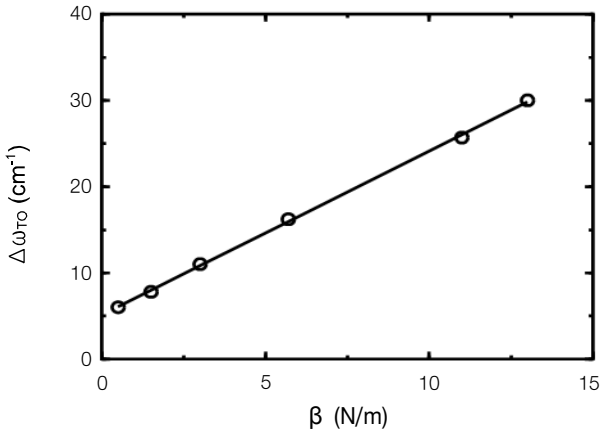

Figure 1. Dependence of simulated pure InAs crystal transverse optical phonon frequency shift ($\Delta\omega_{TO} = \omega_{TO}(\Gamma) - \omega_{TO}(X)$) on $\beta_{\text{In-As-In}}$ parameter. X corresponds to the Brillouin zone-boundary, while Γ to zone-center. $\alpha_{\text{In-As}}$ parameter was varied to satisfy ω_0^h=225.8 cm^{-1} according to Eq. (3) along with $\beta_{\text{In-As-In}}$. An anharmonicity parameter $\chi_{\text{In-As}}$ was kept constant as 1.72 for all points to isolate the TO shift from other effects. Solid line is the least square regression fit of six data points.

temperature limit of the phonon frequency. The parameter $\beta_{\text{In-As-In}}$ mainly controls the downshift of the TO phonon frequency within the Brillouin zone such that one can independently fit $\beta_{\text{In-As-In}}$ using experimentally measured TO shift.[16] The linear dependence of TO shift for pure InAs crystals on $\beta_{\text{In-As-In}}$ is well described in Fig. 1. We have chosen $\beta_{\text{In-As-In}}$ to be 1.5 to have the experimentally measured TO shift of ~5 cm^{-1}.[23] In turn, $\alpha_{\text{In-As}}$ is calculated from Eq. (3) with chosen $\beta_{\text{In-As-In}}$. For alloys, the angular stress between Ga-As-In bonds is determined using the relation $\beta_{Ga-As-In} = \sqrt{\beta_{Ga-As-Ga}\,\beta_{In-As-In}}$.

With a chosen parameter set of $\alpha_{\text{In-As}}$ and $\beta_{\text{In-As-In}}$, the reflectance of pure InAs crystal is calculated. Figure 2 compares the reflectance of InAs obtained by the equation of

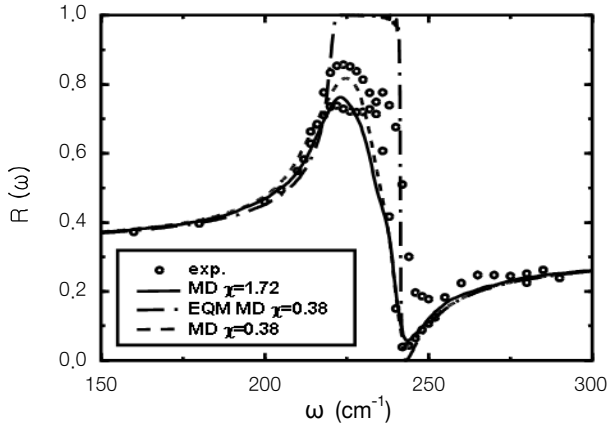

Figure 2. Reflectance $R(\omega)$ of pure InAs crystals. The effect of anharmonicity parameter is well described for pure InAs crystal. Note the change in the Reststrahlen band with different simulation method and the magnitude of $\chi_{\text{In-As}}$. Experimental data are obtained from Ref. 20. MD simulations at room temperature are performed using parameters in Table 1.

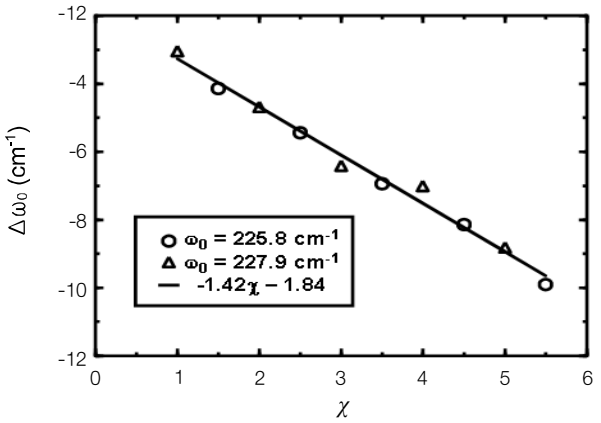

Figure 3. InAs optical phonon frequency shift $\Delta\omega_0 = \omega_0^h - \omega_0^{ah}$ dependence on the dimensionless anharmonicity parameter $\chi_{In\text{-}As}$. To isolate the effect of anharmonicity ω_0^h = 225.8 cm^{-1} (circles) and 227.9 cm^{-1} (triangles) in Eq. (4) were chosen with corresponding $\beta_{In\text{-}As\text{-}In}$ = 1.5. Solid line is the least square regression fit of $\Delta\omega_0$ = −1.42 $\chi_{In\text{-}As}$ −1.84.

motion-molecular dynamics technique (EQM-MD)[24] with experimental results reproduced from dielectric functions in Ref. [25]. It is visible that damping in the simulated reflectance changes with the anharmonicity parameter. By comparing the room temperature MD simulated reflectance spectra and dispersion relations, $\chi_{In\text{-}As}$ = 1.72 has been found to provide better agreement than $\chi_{In\text{-}As}$ = 0.38. $\alpha_{In\text{-}As}$ and $\beta_{In\text{-}As\text{-}In}$ should be adjusted along with $\chi_{In\text{-}As}$. The relation of phonon frequency in Eq. (3) is rewritten as

$$\omega_0^{ah} = \omega_0^h + \Delta\omega_0 \tag{4}$$

where ω_0^{ah} represents the phonon frequency at zone centre obtained from anharmonic Kirkwood-Keating model. From Fig. 3, notice that the linear regression fit of $\Delta\omega_0$ = −1.42 $\chi_{In\text{-}As}$ −1.84 from two different values of ω_0^h (*i.e.*, different sets of $\alpha_{In\text{-}As}$ and $\beta_{In\text{-}As\text{-}In}$); ω_0^h = 225.8 cm^{-1} and 227.9 cm^{-1} with $\beta_{In\text{-}As\text{-}In}$ = 1.5 give essentially the same linear regression relationship. The anharmonicity downshifts optical phonon frequencies such that a bigger $\chi_{In\text{-}As}$ requires a bigger $\alpha_{In\text{-}As}$ to maintain the phonon frequency.

For alloys with only mass disorder, such as $Al_xGa_{1-x}As$, the GaAs- and AlAs-bond have identical charges that can be treated as constant for the whole composition range.[26,27] For $In_xGa_{1-x}As$ alloys, however, the charges at an As atom are 0.71 e and 0.66 e, respectively, in the InAs- and GaAs-bond. One needs a relationship for the charge dependence on composition based on two-end crystal atomic charges. We have used three simple assumptions of the change in atomic charge as a function of composition:

$$q_{eff}(x) = (1-x)q_{eff}^{GaAs} + xq_{eff}^{InAs}, \tag{5}$$

$$[q_{eff}(x)]^2 = (1-x)[q_{eff}^{GaAs}]^2 + x[q_{eff}^{InAs}]^2, \tag{6}$$

$$\frac{\omega_P^2(x)}{\varepsilon_\infty(x)} = (1-x)\frac{(\omega_P^{GaAs})^2}{\varepsilon_\infty^{GaAs}} - x\frac{(\omega_P^{InAs})^2}{\varepsilon_\infty^{InAs}}, \tag{7}$$

The superscript GaAs (InAs) indicates that the value corresponds to GaAs-bond (InAs-bond). The plasma frequency, ω_P, for binary parent crystals, can be evaluated from the Lyddane-Sachs-Teller relation[28]

$$\omega_p^2 = \omega_{LO}^2 - \omega_{TO}^2 = \frac{1}{\Omega\varepsilon_0}\sum_i \frac{(q_{eff}^i)^2}{m_i} \tag{8}$$

where Ω is the volume of the system and m_i is the mass of ion *i*. It was found that the results are insensitive to the choice of assumptions listed above since the charge difference between end crystals is not large and, therefore, we assume that the effective charges $q_{eff}(x)$ depend linearly on composition for the remainder of this article.

In addition, we assume a similar linear dependence of the high frequency dielectric constant and the lattice constant on the composition. The nearest-neighbour distance measured by extended X-ray-absorption fine-structure spectroscopy show that bond lengths in $In_xGa_{1-x}As$ do not follow Vegard's law[29] but remain rather close to their respective values in the pure binary materials.[30] This is naturally supported by the anharmonic Kirkwood-Keating model where the equilibrium distances r_{InAs}^0 (2.62 Å) and r_{GaAs}^0 (2.47 Å) are maintained as constant across the whole composition range. Optimal potential parameters for pure GaAs and InAs crystals are listed in Table 1.

Table 1. Potential parameters for $In_xGa_{1-x}As$

	α, Nm^{-1}	β, Nm^{-1}	χ	(qeff)[a] [q, e]
GaAs	117.7	5.7	1.82	2.15 [0.66]
InAs	106.7	1.5	1.72	2.47 [0.71]

[a] q_{eff} is the effective charge of an As atom in GaAs-bond (InAs-bond) while the atomic charge of a Ga (In) atom is - q_{eff}

Results and Discussion

In this section, we present MD results using previously determined optimal parameters and compare with experimental results. First, the complex dielectric function $\varepsilon(\omega) = \varepsilon'(\omega) + i\varepsilon''(\omega)$ is obtained from the current auto-correlation function; the imaginary part $\varepsilon''(\omega)$ is computed as the following,

$$\varepsilon''(\omega) = \frac{4}{\Omega\omega}\int_0^\tau dt\cos(\omega t)e^{-\sigma\left(\frac{t}{\tau}\right)^2}\left\langle\sum_i q_i\vec{v}_i(t)\sum_j q_j\vec{v}_j(0)\right\rangle, \tag{9}$$

where the angular brackets represent the thermal averaging and the Gaussian damping factor σ was set to 3.0. The real part $\varepsilon'(\omega)$ is obtained through Kramers-Kronig dispersion relation[28] of $\varepsilon''(\omega)$, as given by

$$\varepsilon'(\omega) = \varepsilon_\infty + \frac{1}{\pi}\mathcal{P}\int d(\omega')^2\frac{\varepsilon''(\omega)}{(\omega')^2 - \omega^2} \tag{10}$$

where $\mathcal{P}$ denotes the Cauchy principal value. In Fig. 4, notice the apparent two-mode behaviour in both real and imaginary part of the dielectric functions. While a pure GaAs crystal

exhibits a peak at approximately 265 cm^{-1}, a peak near 225 cm^{-1} starts to develop as the In composition increases (InAs-like peak, hereafter) and the peak near 265 cm^{-1} becomes broader (GaAs-like peak, hereafter). It is clearly seen that the weight of the peak shifts from GaAs-like to InAs-like peak as x increases. Peak positions also shift with atomic composition: the GaAs-like peak moves from 265 to 250 cm^{-1} with x, while the InAs-like peak shifts from 225 to 220 cm^{-1}. While both peaks redshift with x, the GaAs-like peak moves further than the InAs-like one.

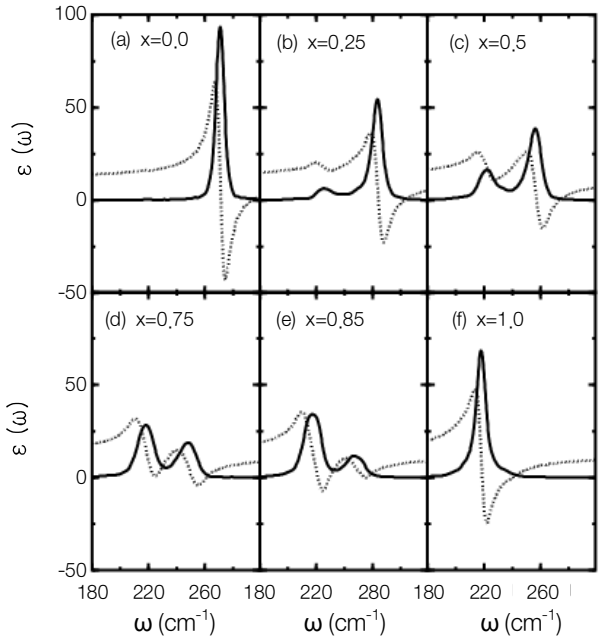

Figure 4. Real (solid line) and imaginary (dotted line) part of dielectric function dependence on composition of $In_xGa_{1-x}As$. (a) pure GaAs, (b) $x = 0.25$, (c) $x = 0.5$, (d) $x = 0.75$, (e) $x = 0.85$, and (f) pure InAs.

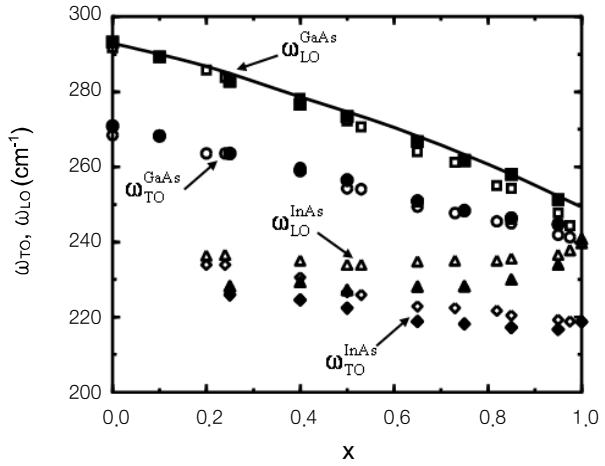

Figure 5. Phonon frequency dependence on composition of $In_xGa_{1-x}As$. Squares are GaAs-like longitudinal, circles are GaAs-like transverse, triangles are InAs-like longitudinal, and diamonds are InAs-like transverse optical modes. Hollow markers are from experimental results in Ref. 6 and solid markers are from MD simulations at room temperature using parameters in Table 1. Solid line is Shen's second order equation $\omega_{LO}^{GaAs} = -16.5x^2 - 26.7x + 292.3$ for GaAs-like LO phone frequency dependence on x.[13]

Figure 5 compares experimentally obtained[8] and simulated optical phonon frequencies as a function of composition. The phonon frequency varies with composition due to the coupling to macroscopic electric fields and the statistically averaged forces between the atoms, which depend on the fluctuations of local configurations. While TO frequencies evolve almost linearly with x, GaAs-like and InAs-like LO frequencies, ω_{LO}^{GaAs} and ω_{LO}^{InAs}, display positive and negative bowing, respectively. According to Shen *et al.,* the GaAs-like LO phonon can be fitted to the second-order equation of x such that $\omega_{LO}^{GaAs} = -16.5x^2 - 26.7x + 292.3$,[12] which appears in Fig. 5 as a solid line. Simulated results agree well with Shen's second-order relation and experimental data.

We also calculated Raman spectra as follows,[31] which are plotted in Fig. 6:

$$I(\omega) \propto -\mathrm{Im}\left[\frac{1}{\varepsilon(\omega)}\right] = \frac{\varepsilon''(\omega)}{\varepsilon'(\omega)^2 + \varepsilon''(\omega)^2} \,. \tag{11}$$

Note a strong GaAs-like peak, even when the fraction of GaAs is smaller than 0.5. It is also interesting that, the weight of the GaAs-like LO mode is as intense as that of the InAs-like one even with the fraction of GaAs as small as 0.05. To analyze the Raman spectrum in a more comprehensive manner, we fit Raman peaks with a Lorentzian lineshape that is shown in a dotted line in Fig. 6:

$$I(\omega) = \frac{\tilde{I}}{1 + 4(\omega - \tilde{\omega})^2 / \Gamma^2} \,. \tag{12}$$

Here, $\tilde{\omega}$ is a resonant frequency, i.e., LO frequency, $\tilde{I}$ is the intensity of the Raman peak at $\tilde{\omega}$. In order to emphasize the two-mode behaviour of the mixed alloys and to estimate

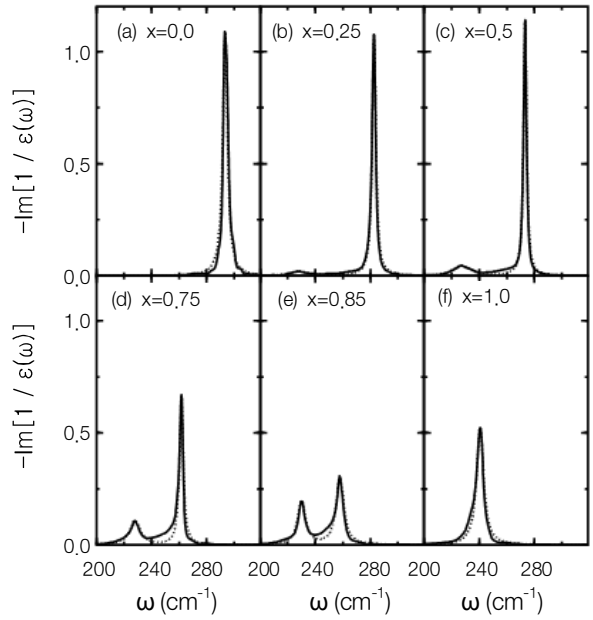

Figure 6. Raman peaks dependence on composition of $In_xGa_{1-x}As$. (a) pure GaAs, (b) $x = 0.25$, (c) $x = 0.5$, (d) $x = 0.75$, (e) $x = 0.85$, and (f) pure InAs. The sum of two separate Lorentzian lineshape fits of GaAs- and InAs-like is shown as dotted lines.

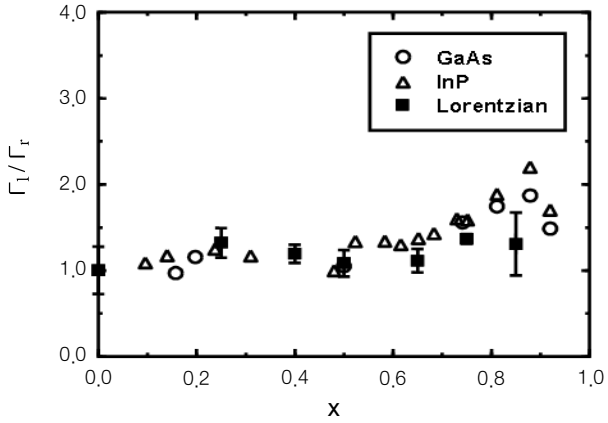

Figure 7. Asymmetric width ratio Γ_l/Γ_r of FWHM of GaAs-like Raman peaks of $In_xGa_{1-x}As$. Hollow circles and triangles are experimental results of $In_xGa_{1-x}As$/GaAs and $In_xGa_{1-x}As$/InP, respectively, which are reported in Ref. [13]. Solid squares are MD results using parameters in Table 1. FWHM were obtained from the least square regression Lorentzian lineshape fit in Fig. 6.

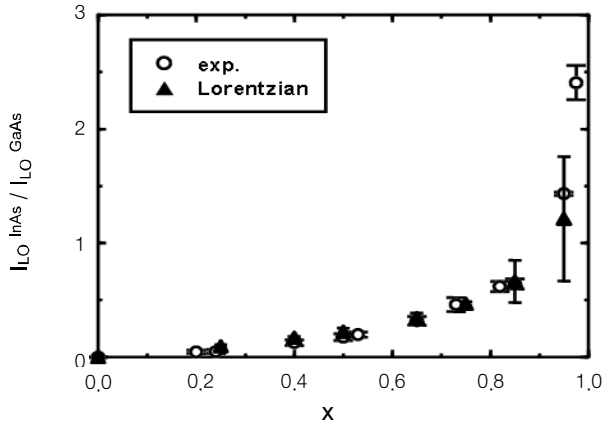

Figure 8. Longitudinal optical phonon mode intensity ratio between InAs-like and Ga-like Raman peaks. Experimental results (hollow circles) are reproduced from Ref. [9]. Simulation intensities are obtained by integrating Lorentzian lineshapes in Fig. 6.

the relative intensity of the modes, we separated the Raman peak of mixed alloys into corresponding binary parent crystal-like modes. Simulated data are broken at 240 cm^{-1} into two modes: high-frequency peak corresponds to the GaAs-like mode, while the low-frequency peak to InAs-like mode. High- and low-frequency peaks are, then, independently fitted to Lorentzian functions by means of the least-square regression. By comparing simulated Raman peaks and fitted Lorentzian lineshapes toward In-rich region, the sum of two Lorentzian peaks deviates from simulated results, especially in the frequency range between 230 ~ 255 cm^{-1}. This implies that there is more interaction between GaAs-like and InAs-like LO modes as In concentration becomes higher. Due to the intensity build up, the standard deviation of the Lorentzian fit becomes large. Error bars in Figs. 7 and 8 indicate the difference between MD simulation results and the fitted Lorentzian lineshapes in Fig. 6.

It has been known that the finite spatial phonon mode correlation length owing to the potential fluctuation of the alloy disorder led to the broadening and asymmetry of the Raman line shape.[32] In Fig. 7, we present the asymmetric width ratio Γ_l/Γ_r of the full-width half maximum (FWHM) of GaAs-like Raman peaks. Excellent agreement was achieved by comparison with the experimental observation reported in Ref. 8, where the subscript l(r) indicates the left (right) half-side of the Raman peak. It has been shown that Raman peaks are independent of local configurations because corresponding frequency fluctuations are not large enough to produce phonon localization.[33,34] Therefore, by randomly choosing Ga and In atomic sites, one local configuration is enough to study Raman scattering spectra. In addition, it has been speculated that the substrate and the plastic relaxation might have played a significant role for the linewidth and profile of the Raman peaks.[9-12] The absence of the substrate and plastic relaxation in our (computer experimented) sample may have caused the discrepancy between simulated and experimental results in Fig. 7. Finally, Fig. 8 shows an InAs-like/GaAs-like LO intensity ratio. One can observe increase of the GaAs-like Raman peak intensity at the expense of that of the InAs-like one. The GaAs-like LO intensity remains higher than that of the InAs-like LO, until x exceeds 0.95.

Concluding Remarks

In this article, we have modelled $In_xGa_{1-x}As$ with arbitrary atomic composition using the anharmonic Kirkwood-Keating potential with a Morse strain energy. In order to describe the compositional dependence of parameters, we have varied effective charges, high frequency dielectric constants and lattice constants based on the linear relationship. It has been shown that the optical-phonon behaviour of $In_xGa_{1-x}As$ is affected by three main effects: mass disorder, microscopic relaxation, and coupling by the ionic polarization field. While mass disorder and microscopic relaxation are represented by the Kirkwood-Keating strain energy, the ionic polarization field is taken into account by Coulomb interaction. With a selected set of optimal potential parameters, experimentally measured dispersion relations, dielectric functions, and Raman-scattering spectra were accurately reproduced.

For MD simulations performed in this article, we have intentionally mixed lattice sites of gallium and indium at random and found that parameterization process required the properties of binary parent crystals regardless of the details of the local structure. Therefore, the model can also be applied to other semiconductor based materials with complicated quantum well heterostructures. In particular, the model system is expected to provide a valid and effective theoretical tool to design semiconductor quantum well structures that exhibit desired optical properties of various QDs. In future work, the results of this study will be extended to design and investigate quantum well structures including core/shell heterostructures that consist of GaAs and InAs layers with various thickness profiles. It should be noted, however, that the surface interactions, negligible in alloy forms, is substantial in a QD and, in turn, might alter the optical properties of QDs significantly. Further investigations relevant to the surface relaxation are currently underway.

Acknowledgments. This work was supported by the Korea Science and Engineering Foundation (KOSEF-R01-2007-000-11831-0) and by the Ministry of Education and Human Resources Development (MOEHRD) (KRF-2007-313-C00350) in which part of calculations were performed by using the supercomputing resource of the Korea Institute of Science and Technology Information (KISTI). MH thanks the fellowship of the BK 21 program from MOEHRD.

References

1. Kim, S.; Lim, Y. T.; Soltesz, E. G.; DeGrand, A. M.; Lee, J. Nakayama, A.; Parker, J. A.; Mihaljevic, T.; Laurence, R. G.; Dor, D. M.; Cohn, L. H.; Bawendi, M. G.; Frangioni, J. V. *Nature Biotechnology* **2004**, *22*, 93.
2. Kim, S.-W.; Zimmer, J. P.; Ohnishi, S.; Tracy, J. B.; Frangioni, J. V.; Bawendi, M. G. *J. Am. Chem. Soc*. **2005**, *127*, 10526.
3. Troccoli, M.; Belyanin, A.; Capasso, F.; Cubukcu, E.; Sivco, D. L.; Cho, A. Y. *Nature* **2005**, *433*, 845.
4. Elia, A.; Lugara, P. M. ; Giancaspro, C. *Opt. Lett.* **2005**, *30*, 988.
5. Krenner, H. J.; Stufler, S.; Sabathil, M.; Clark, E. C.; Ester, P.; Bichler, M.; Abstreiter, G.; Finley, J.; Zrenner, A. *New J. Phys.* **2005**, *7*, 184.
6. Kim, E.-T.; Madhukar, A.; Ye, Z.; Campbell, J. C. *Appl. Phys. Lett.* **2004**, *84,* 3277.
7. Razeghi, M.; Slivken, S. *Opto-Elect. Rev.* **2003**, *11*, 85.
8. Groenen, J.; Carles, R.; Landa, G.; Guerret-Piécourt, C.; Fontaine, C.; Gendry, M. *Phys. Rev. B* **1998**, *58*, 10452.
9. Soni, R. K. *J. Cryst. Growth* **1989**, *94*, 347.
10. Jusserand, B.; Sapriel, *J. Phys. Rev. B* **1981**, *24*, 7194.
11. Manor, R.; Brafman, O.; Fekete, D.; Sarfaty, R. *Phys. Rev. B* **1993**, *47*, 9492.
12. Shen, J. L.; Chang, I. M.; Shu, Y. M.; Chen, Y. F.; Chang, S. Z.; Lee, S. C. *Phys. Rev. B* **1994**, *50*, 1678.
13. Baroni, S.; de Gironcoli, S.; Giannozzi, P. *Phys. Rev. Lett.* **1990**, *65*, 84.
14. Jusserand, B.; Mollot, F.; Planel, R.; Molinary, E.; Baroni, S. *Surf. Sci.* **1992**, *267*, 171.
15. Bonneville, B. *Phys. Rev. B* **1981**, *24*, 1987.
16. Sim, E.; Beckers, J.; de Leeuw, S. W.; Thorpe, M. F.; Ratner, M. A. *J. Chem. Phys.* **2005**, *122*, 174702.
17. Kirkwood, J. G. *J. Chem. Phys*. **1939**, *7*, 506.
18. Keating, P. N. *Phys. Rev.* **1966**, *145*, 637.
19. Yu, P. Y.; Cardona, M. *Fundamentals of Semiconductors*; Springer-Verlag: Berlin, 1996.
20. Ewald, P. *Ann. Phys.* **1921**, *64*, 253.
21. Pollock, E. L.; Glosli, J. *Comp. Phys. Commun.* **1996**, *95*, 93.
22. Cai, Y.; Thorpe, M. F. *Phys. Rev. B* **1992**, *46*, 15872; 15879.
23. Poerschke, R. *Semiconductors: Group IV Elements and III-V Compounds*; Madelung, O., Ed.; Springer-Verlag: New York, 1991.
24. Thorpe, M. F.; de Leeuw, S. W. *Phys. Rev. B* **1986**, *33*, 8490.
25. *Handbook of Optical Constants of Solids*; Palik, E. D., Ed.; Academic Press: Boston, 1985.
26. Bernasconi, M.; Colombo, L.; Miglio, L.; Benedek, G. *Phys. Rev. B* **1991**, *43*, 14447.
27. Kim, O. K.; Spitzer, W. G. *J. Appl. Phys.* **1979**, *50*, 4362.
28. Elliott, R. J.; Krumhansl, J. A.; Leath, P. L. *Rev. Mod. Phys.* **1971**, *46*, 465.
29. Vegard, L. *Z. Phys.* **1921**, *5*, 17.
30. Balzarotti, A.; Motta, N.; Kisiel, A.; Zimnal-Starnawska, M.; Czyzyk, M. T.; Podgórny, M. *Phys. Rev. B* **1985**, *31*, 7526.
31. Look at any introductory solid state physics book, such as Kittel, C. *Introduction to Solid State Physics*, 5th ed.; John Wiley & Sons: New York, 1976.
32. Richter, H.; Wang, Z. P.; Ley, L. *Solid State Commun.* **1981**, *39*, 625.
33. Fuchs, H. D.; Etchegoin, P.; Cardona, M.; Itoh, K.; Haller, E. E. *Phys. Rev. Lett.* **1993**, *70*, 1715.
34. Zhang, J. M.; Giehler, M.; Göbel, A.; Ruf, T.; Cardona, M.; Haller, E. E.; Itoh, K. *Phys. Rev. B* **1998**, *57*, 1348.